第 24 卷第 5 期 无 机 化 学 学 报 Vol.24 No.5
2008 年 5 月 CHINESE JOURNAL OF INORGANIC CHEMISTRY 797~802

# 多层多孔 $Co_3O_4$ 纳米粒子组装体的合成、表征和电化学性能研究

韩 敏[1] 张文莉[1] 石乃恩[1] 李景虹[2] 徐 正*,[1]
([1]南京大学化学化工学院配位化学国家重点实验室,南京 210093)
([2]清华大学化学系,北京 100084)

**摘要**: 利用十二烷基磺酸钠(SDS)作为表面活性剂,合成了形貌化的 $CoC_2O_4$ 配合物前驱物,然后在 500 ℃下热分解形貌化的前驱物,得到了多层多孔 $Co_3O_4$ 纳米粒子组装体。采用 FESEM、TEM、HRTEM、XRD、$N_2$ 吸附脱附和 Raman 散射等手段对产物进行了分析和表征。低角 XRD,TEM 和 $N_2$ 吸附脱附测试表明所得组装体具有多孔结构。常规 XRD、HRTEM 和 Raman 结果证明组装体中 $Co_3O_4$ 纳米粒子建筑块结晶较好。与体相 $Co_3O_4$ 晶体相比,$Co_3O_4$ 纳米粒子组装体的 5 个拉曼活性峰发生了明显的红移。将 $Co_3O_4$ 纳米粒子组装体作为锂离子电池的正极材料进行了电化学性能测试, 结果表明该组装体电极的首次放电容量为 1 115 mAh·g$^{-1}$,远高于目前文献报道的 $Co_3O_4$ 纳米管、纳米粒子和纳米棒电极。但是,该组装体电极的循环性能不好,有待进一步提高。

**关键词**: $Co_3O_4$; 纳米粒子组装体; 电化学性质
**中图分类号**: O611.62; O614.81+2; O646.21 **文献标识码**: A **文章编号**: 1001-4861(2008)05-0797-06

# Synthesis, Characterization and Electrochemical Properties of Multi-layered Porous $Co_3O_4$ Nanoparticle Assemblies

HAN Min[1] ZHANG Wen-Li[1] SHI Nai-En[1] LI Jing-Hong[2] XU Zheng*,[1]
([1]*State Key Laboratory of Coordination Chemistry, School of Chemistry and Chemical Engineering, Nanjing University, Nanjing* 210093)
([2]*Department of Chemistry, Tsing Hua University, Beijing* 100084)

**Abstract:** Multi-layered $Co_3O_4$ nanoparticle assemblies with well arranged $Co_3O_4$ nanoparticles have been fabricated through thermal conversion of micelle-assisted shaped precursor. Low angle diffraction data, TEM images and nitrogen-adsorption studies show that the obtained assemblies are porous. Wide angle XRD, HRTEM and Raman analysis results exhibit that the $Co_3O_4$ nanoparticle building blocks are well crystallized. Corresponding Raman spectrum of the assemblies shifts toward low wave number region compared with that for bulk crystalline $Co_3O_4$. Electrochemical measurement results demonstrate that the obtained $Co_3O_4$ nanoparticle assemblies can be served as a good cathode material for lithium secondary batteries. The initial discharge capacity of the electrode made from $Co_3O_4$ nanoparticle assemblies is 1 115 mAh·g$^{-1}$, which is much higher than that of the reported $Co_3O_4$ nanotubes, nanoparticles and nanorods electrodes. However, its cycling performance and stability are to be improved.

**Key words:** $Co_3O_4$; nanoparticle assemblies; electrochemical properties

Advanced architecture of complex nanostructures is desirable because of their potential applications in photonics, catalytic supports, biological labeling and electronic devices [1]. The construction of complex

收稿日期:2007-12-13。收修改稿日期:2008-01-25。
国家自然科学基金(No.90606005 and No.20490210)资助项目。
*通讯联系人。E-mail:zhengxu@netra.nju.edu.cn
第一作者:韩 敏,男,29 岁,博士后;研究方向:低维纳米材料的可控合成、组装与性能研究。

supramolecular nanostructures from organic compounds by the self assembly route has been reported through non-covalent interactions such as Van der Waals forces, $\pi$-$\pi$ interactions, hydrogen bonding, electro-static forces, metal-ligand coordination and host-guest interactions[2]. Using similar interactions, metal nanoparticles (Au, Ag, FePt, etc)[3] and some semiconductor nanoparticles(CdSe, CdS, etc)[4] have been integrated to various 1D (1-dimensional), 2D and 3D nanostructur-es. This approach can also be extended to organize oxide nanoparticles[5]. For example, magnetite nanocry-stals have been assembled into 3D spherical aggregates via the inclusion interactions of $\beta$-Cyclodextrins. Using this strategy, the size and geometrical structure of the desired product can be tunable by controlling the functional groups adsorbed on its surface, but this will bring impurities of organic molecules into the final product, which may affect the performance of the materials. Therefore, exploring an effective method for producing and assembling pure nanoscaled functional building units into advanced architectures is necessary and continues to be a key challenge in current material synthetic fields.

As an important group in transition metal oxides, $Co_3O_4$ nanomaterials have attracted much attention in recent years[6~12] because they show some interesting magnetic, optical, transport, electrochemical and field-emission properties, which may find potential applications in sensors, catalysis, energy storage in secondary batteries and flat panel display devices[12~17]. Up to now, various $Co_3O_4$ nanostructure building blocks have been synthesized via different synthetic methods. However, few works have been reported on organizing those nanoscaled functional building blocks into complicated architectures[18,19]. Here, we report a facile and effective fabrication method for in situ organizing pure $Co_3O_4$ nanoparticles into 3D multi-layered porous structure.

## 1 Experimental

### 1.1 Synthesis of Multi-layered Porous $Co_3O_4$ Nanoparticle Assemblies

In a typical synthesis procedure, 2 mmol $CoCl_2 \cdot 6H_2O$ and 2 mmol sodium dodecylsulfate (SDS) were added in 50 mL deionized water. A red solution was formed. Then, 50 mL aqueous solution containing 4 mmol $(NH_4)_2C_2O_4$ and 2 mmol SDS was added to the red solution quickly. The mixture was heated in an oil bath at 50 ℃ for 4 h under magnetic stirring. The precipitate was collected by centrifugation and washed with deionized water for several times to remove the raw materials and by-products. Finally, the precipitate was dried under vacuum at ambient temperature, which is used for thermal treatment to obtain the desired product.

The synthesized precursor powder was placed in an alumina boat and then put this boat in the central area of a horizontal tube furnace. The tube furnace was heated to 500 ℃ at a rate of 1.5 ℃·min$^{-1}$ and kept at that temperature for 2 h. Subsequently, the furnace was cooled down to room temperature at a rate of 2 ℃·min$^{-1}$. The black product in the boat was collected and used for characterization.

### 1.2 Characterization of Multi-layered Porous $Co_3O_4$ Nanoparticle Assemblies

Field emission scanning electron microscopy (FE-SEM) images were taken on a LEO-1530VP scanning electron microscope, operating at an accelerating voltage of 20 kV. Powder X-Ray diffraction measurements were performed on an XPert Pro MPD diffractometer (PANalytical) using Ni-filtered Cu $K\alpha$ radiation ($\lambda_{K\alpha 1}$=0.154 06 nm), Hybird monochromators, and X Celerator detector. Corresponding work voltage and current were 40 kV and 40 mA, respectively. The High-Score Software was used to peel off the Cu $K\alpha_2$ radiation and deal with the acquired diffraction data. The transmission electron microscopy (TEM) images were taken on a JEM-200CX instrument (Japan), using an accelerating voltage of 200 kV. High-Resolution transmission electron microscopy(HRTEM) images were obtained on JEOL-2010 at an accelerating voltage of 200 kV. Nitrogen-adsorption and -desorption isotherms were measured with a Micromeritics Tristar 3000 system. Raman spectrum was recorded on JY HR800 (France) instrument with an optical multichannel spectrometer Microdil 28(Dilor) equipped with a micro-

scope. An objective with x 100 magnification was used both for focusing the excitation light ($Ar^+$ laser, 488 nm) and for collecting the scattered light.

### 1.3 Electrochemical measurements

Galvanostatic measurements were carried out using two-electrode cells with lithium metal as the counter electrode. The working electrodes were fabricated by compressing the mixture of 80wt% active materials, 10wt% acetylene black, and 10wt% ploytetrafluoroethylene (PTFE) onto an aluminum foil. The pellets of the same mass were dried in vacuum at 100 ℃ for at least 8 h and then assembled as cells in an Ar-filled Labconco glovebox. The electrolyte solution was 1 mol·$L^{-1}$ $LiPF_6$ dissolved in a mixture of ethylene carbonate (EC), dimethyl carbonate (DMC), and diethyl carbonate (DEC) with the volume ratio of EC∶DMC∶DEC=1∶1∶1. Voltage-capacity plots were recorded from 3.0 and 0.1 V at a current density of 0.2 mA·$cm^{-2}$ using a Roofer Battery Tester(Shenzhen, China).

## 2 Results and discussion

### 2.1 Morphology analysis of the complex precursor

SDS is a useful surfactant(CMC is 0.008 7 mol·$L^{-1}$) and widely used in the synthesis of nanomaterials and mesoporous materials. Our results show that the concentration of SDS has great impact on the shape of the complex precursor. Fig.1 shows the FESEM images of the complex precursor when the concentration of SDS is set at 0.04 mol·$L^{-1}$. From the low magnification FESEM image shown in Fig.1a, large area complicated tetragonal-prism-like structures with hollow interior can be observed. Corresponding high magnification FESEM image is shown in Fig.1b.

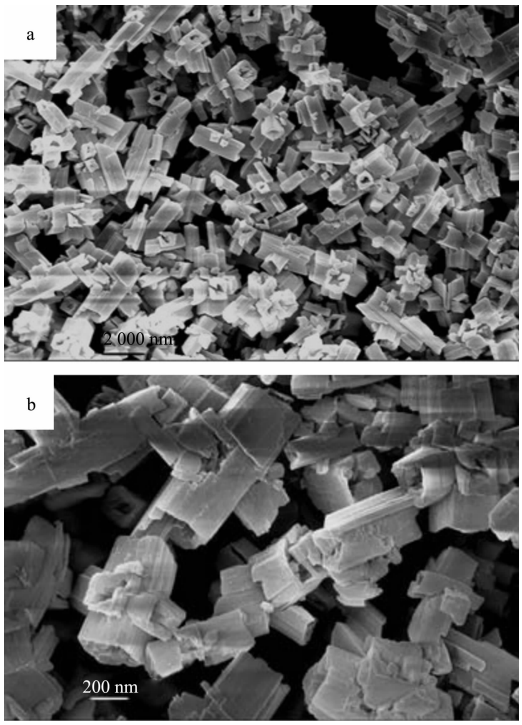


Fig.1 FESEM images of the complex precursors synthesized at 0.04 mol·$L^{-1}$ SDS. (a) Large area low magnification FESEM image. (b) Corresponding high magnification FESEM image

### 2.2 Morphology and microstructure analysis of the $Co_3O_4$ nanoparticle assemblies

After thermal treatment of the shaped precursor at 500 ℃ for 2 h, multi-layered(ML) $Co_3O_4$ microstructures will be obtained. Corresponding FESEM images are shown in Fig.2. Fig.2a exhibits the low magnification FESEM image of the ML $Co_3O_4$ microstructures. In comparison with the precursor (Fig.1), a part of the product retains its figuration, but some of them are collapsed and splitted into belt-like nanostructures during the thermal conversion. From the corresponding high magnification FESEM images shown in Fig.2b~2d, we can see that many small nanoparticles are self-assembled into nanochains and then the nanochains are organized into a rectangle-like plane, which stacks into a ML structure with rectangle cross section. Furthermore, the interspacing between the neighboring

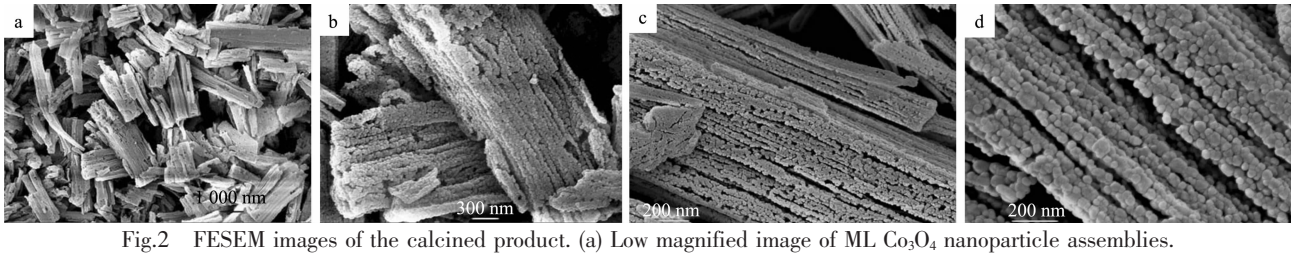


Fig.2 FESEM images of the calcined product. (a) Low magnified image of ML $Co_3O_4$ nanoparticle assemblies. (b), (c) and (d) are the corresponding high magnification images of the nanoparticle assemblies

nanoparticle chains can also be observed. The detailed mechanism on the formation of such nanoparticle assemblies is not fully clear at present and further work on this is underway.

The morphology and microstructure of the ML $Co_3O_4$ nanoparticle assemblies are further examined by transmission electron microscopy (TEM) and high resolution transmission electron microscopy (HRTEM). From the TEM image shown in Fig.3a, we can see that the assemblies are composed of small polygon nanoparticles. The corresponding HRTEM image (Fig.3b) of the rectangle area in Fig.3a shows clear 2D atomic lattice fringes. The lattice spacing of 0.472 nm is corresponding to the spacing of (111) planes of cubic phase $Co_3O_4$. HRTEM result indicates that the nanoparticle building blocks are well crystallined.

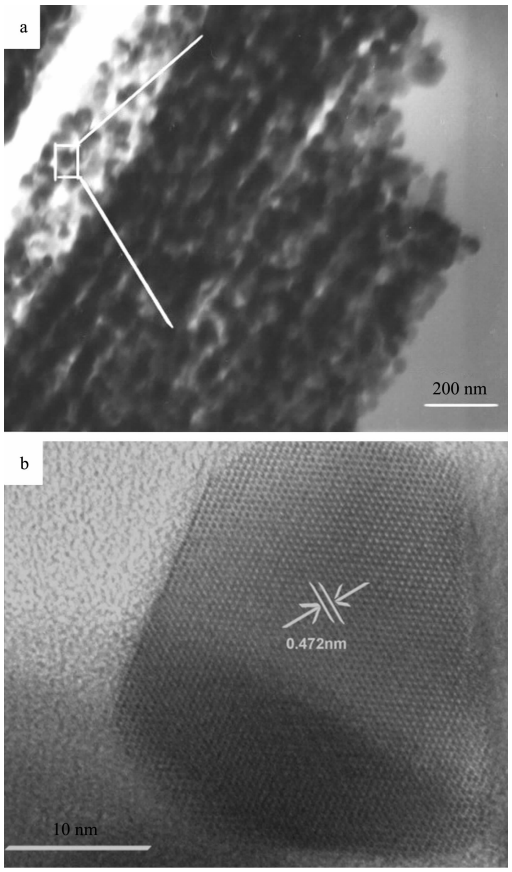


Fig.3 (a) TEM image of the ML $Co_3O_4$ nanoparticle assemblies. (b) Corresponding high resolution TEM image of the selected area in(a)

## 2.3 XRD and nitrogen adsorption-desorption studies of the $Co_3O_4$ nanoparticle assemblies

Powder X-ray diffraction pattern of the ML $Co_3O_4$ nanoparticle assemblies is shown in Fig.4a. All the peaks can be indexed as the (111), (220), (311), (222), (400), (511) and (440) planes of cubic phase $Co_3O_4$(PDF No.42-1467). The XRD result shows that the obtained nanoparticle architectures are well crystallined, further confirming the HRTEM result. Corresponding low angle X-Ray diffraction data of the assemblies is presented in Fig.4b. It shows that a sharp and well-resolved, high-intensity diffraction peak appears at 0.536°, suggesting an ordered mesostructure in the assemblies. Further evidence comes from the nitrogen-adsorption study. A typical type-Ⅳ adsorption-desorption isotherm plot with hysteresis is clearly observed in Fig.4c, strongly confirming the porous character of assemblies. BJH desorption pore size distribution plot shown in the inset of Fig.4c demonstrates that the average pore diameter of the assemblies is 37 nm.

## 2.4 Raman scattering analysis of the $Co_3O_4$ nanoparticle assemblies

Fig.4d shows the Raman spectrum of the ML porous $Co_3O_4$ nanoparticle assemblies sample on a glass slide excited by a 488 nm $Ar^+$ laser. Five distinct Raman peaks centered at 191, 473, 514, 609 and

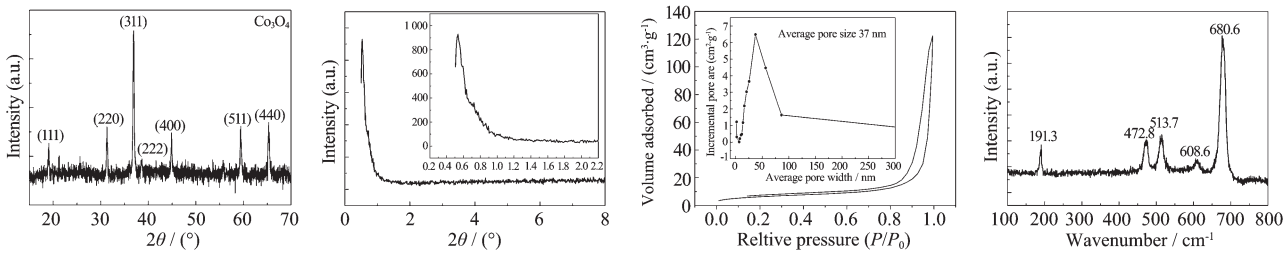


Fig.4 (a) XRD pattern of the ML porous $Co_3O_4$ nanoparticle assemblies. (b) Corresponding low angel XRD pattern of the assemblies. (c) Nitrogen-adsorption measurement: Isotherm linear plot of the ML $Co_3O_4$ nanoparticle assemblies, inset is the corresponding BJH desorption pore size distribution curve. (d) Raman spectrum of the ML porous $Co_3O_4$ nanoparticle assemblies

681 $cm^{-1}$ are clearly observed, which can be indexed as $F_{2g}^{1}$, $E_g$, $F_{2g}^{2}$, $F_{2g}^{3}$, and $A_{1g}$ modes of the crystalline $Co_3O_4$, respectively. Compared with that for bulk $Co_3O_4$, the peak positions of the five active modes are red shifted about 3, 10, 8, 10 and 10 $cm^{-1}$, respectively [20]. This red shift phenomenon is attributed to the optical phonon confinement effect in nanostructures that can cause uncertainty in the phonon wave vectors and then a downshift of the Raman peaks[21,22].

### 2.5 Electrochemical properties of the $Co_3O_4$ nanoparticle assemblies

Because the $Co_3O_4$ nanoparticle assemblies possess multilayer-like and porous microstructure, which are beneficial to the diffusion of Li ions, a cell configuration of $Co_3O_4$/Li is made to investigate their electrochemical properties. Fig.5a shows the first and second discharge-charge cycles plots of the electrode made from ML porous $Co_3O_4$ nanoparticle assemblies at a current density of 0.2 mA·$cm^{-2}$ in the 3.0~0.1 V potential window. The first cycle discharge curve exhibits a high discharging voltage(2.3 V) and a very long plateau, indicating a high power-output behaviour. The first cycle discharge capacity of the $Co_3O_4$ nanoparticle assemblies electrode is 1 115 mAh·$g^{-1}$, which is much higher than that of the reported $Co_3O_4$ nanotubes (850 mAh·$g^{-1}$), $Co_3O_4$ nanoparticles(830 mAh·$g^{-1}$) and $Co_3O_4$ nanorods(815 mAh·$g^{-1}$) electrodes [16]. The contribution of the reaction of lithium with carbon additive is at a magnitude of 60 mAh·$g^{-1}$, and is thus not take into account for such high specific capacity [19a]. The whole electrochemical reaction can be written as follows:

$$Co_3O_4 + 8Li^+ + 8e^- \underset{\text{Charge}}{\overset{\text{Discharge}}{\rightleftharpoons}} 3Co + 4Li_2O$$

The extra capacity can be associated with the presence of the redox process involving the electrolyte [19a]. Subsequently, almost eight lithium should be reversibly intercalated/deintercalated. However, the cycle performance of the $Co_3O_4$ nanoparticle assemblies electrode shown in Fig.5b is not satisfactory, indicating that the intercalation and deintercalation of lithium in our electrode are not completely reversible. Starting from the first cycle, the discharge capacity decreases with increasing cycles. The rate of the capacity decay from the first to the fifth cycle is much higher than that from the fifth to the forty-fifth cycle. After forty five cycles, the nanoparticle assemblies electrode maintains about 200 mAh·$g^{-1}$, corresponding to about 20% of the initial capacity. The relative high capacity decay rate may be attributed to microstructure change during the numerous charge-discharge cycles, which affects the intercalation/deintercalation of the lithium ion and the final electrochemical behaviour of the sample. The detailed mechanism on the discharge process and capacity decay is not clear at present. Further work on this issue is in progress in this laboratory.

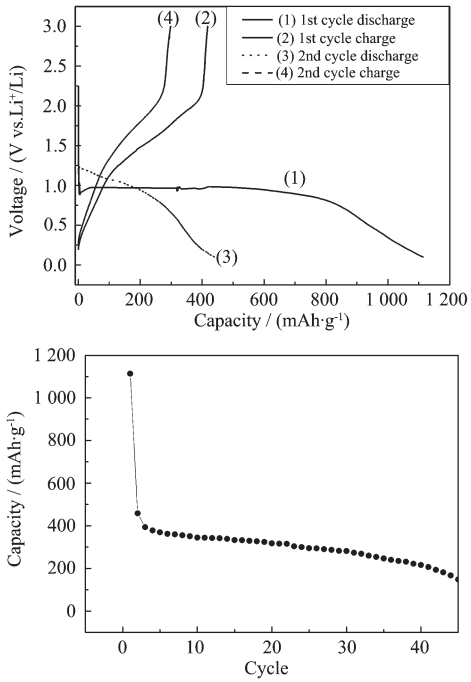


Fig.5 (a) Voltage-capacity plots for ML porous $Co_3O_4$ nanoparticle assemblies at a current density of 0.2 mA·$cm^{-2}$ in the 3.0~0.1 V potential window for the first and second discharge-charge cycles. (b) Cycling performance of $Co_3O_4$ nanoarchitectures at a current density of 0.2 mA·$cm^{-2}$ in the 3.0~0.1 V potential window

## 3 Conclusions

In summary, ML porous $Co_3O_4$ nanoparticle assemblies have been fabricated via thermal conversion of micelle-assisted shaped precursor. Low angle X-ray diffraction data and nitrogen-adsorption studies show that the assemblies are porous. Corresponding XRD,

HRTEM and Raman analysis results exhibit that $Co_3O_4$ nanoparticle building blocks are well crystallined. Compared with the bulk crystalline $Co_3O_4$, the Raman spectrum of the $Co_3O_4$ nanoparticle assemblies shifts toward low wave number region. Galvanostatic measurement results demonstrate that the obtained porous $Co_3O_4$ nanoparticle assemblies possess good electrochemical properties.

## References:


[1] (a) Wijnhoven J E G J, Vos W L. *Science*, **1998**,**281**:802~804
(b) Wang H Z, Uehara M, Nakamura H, et al. *Adv. Mater.*,**2005**, **17**:2506~2509

[2] Shimizu T, Masuda M, Minamikawa H. *Chem. Rev.*, **2005**,**105**: 1401~1443.

[3] (a) Shi N E, Yin G, Xu Z, et al. *Chem. Lett.*, **2005**,**34**:1468~ 1469
(b) Liz-Marzan L M. *Langmiur*, **2006**,**22**:32~41
(c) Sun S H. Adv. Mater., **2006**,**18**:393~403

[4] Tang Z Y, Kotov N A. Adv. Mater., **2005**,**17**:951~962

[5] (a) Chen H, Gu J, Gao J, et al. *Adv. Mater.*, **2005**,**17**:2010~ 2013
(b) Polleux J, Pinna N, Niederberger M, et al. *Adv. Mater.*,2004, 16:436~439
(c) Hou Y L, Kondoh H, Sako E O, et al. *J. Phys. Chem. B*, **2005**,**109**:19094~19098

[6] Nethravathi C, Sen S, Harbrecht B, et al. *J. Phys. Chem. B*, **2005**,**109**:11468~11472

[7] Liu Y K, Wang G H, Xu C K, et al. *Chem. Commun.*, **2002**,**14**: 1486~1487

[8] Guan H Y, Shao C L, Wen S B, et al. *Mater. Chem. Phys.*, **2003**,**82**:1002~1006

[9] (a)Xu R, Zeng H C. *J. Phys. Chem. B*, **2003**,**107**:926~930
(b)Feng J, Zeng H C. *Chem. Mater.*, **2003**,**15**:2829~2835

[10] (a)Shi X Y, Han S B, Zhou F M, et al. *Nano Lett.*, **2002**, **2**:289~293
(b)Li T, Yang S G, Du Y W, et al. *Nanotech.*, **2004**,**15**:1479~ 1482

[11]Wang Y Q, Yang C M, Schüth F, et al. *Adv. Mater.*, **2005**,**17**: 53~56

[12]Yu T, Zhu Y W, Sow C H, et al. *Adv. Mater.*, **2005**,**17**:1595~ 1599

[13]Takada S, Fujii M, Kohiki S, et al. *Nano Lett.*, **2001**,**1**:379 ~382

[14]Yamamoto H, Tanaka S, Naito T, et al. *Appl. Phys. Lett.*, **2002**,**81**:999~1001

[15]Tejada J, Zhang X X, del Barco E, et al. *Phys. Rev. Lett.*, **1997**,**79**:1754~1757

[16]Li W Y, Xu L N, Chen J. *Adv. Func. Mater.*, **2005**,**15**:851~857

[17]Shan Y, Gao L. *Chem. Lett.*, **2004**,**33**:1560~1561

[18]Xu R, Zeng H C. *J. Phys. Chem. B*, **2003**,**107**:12643~12649

[19](a)Wang X, Chen X Y, Zhang Z D, et al. *J. Phys. Chem. B*, **2004**,**108**:16401~16404
(b)He T, Chen D R, Jiao X L. *Chem. Mater.*, 2004,16:737~743

[20]Hadjiev V G, Iliev M N, Vergilov I V. *J. Phys. C: Solid State Phys.*, **1988**,**21**:L199~L201

[21]Cao B Q, Cai W P, Duan G T, et al. *Nanotech.*, **2005**,**16**:2567 ~2574

[22]Du Y, Zhang M S, Hong J, et al. *Appl. Phys. A-Mater. Sci. Proc.*, **2003**,**76**:171~176